Microrheology

Juan Ruben Gomez-Solano

September 27, 2019

0.1 Microrheology

Microrheology is one of the most widespread applications of optical tweezers in Soft Matter Physics. It comprises a number of experimental techniques that allow to investigate the mechanical response of soft materials such as simple liquids, polymer solutions, micellar fluids, colloidal suspensions, liquid crystals, and gels, using colloidal particles as micron-sized probes [1, 2, 3]. Similar to bulk rheology, microrheology is concerned with flow and deformation of such materials under applied stress or strain. Depending on the specific details of their microstructure, different kinds of rheological behavior can be observed. For instance, for most simple liquids, the rheological response is *Newtonian*: upon imposing a given strain rate, the resulting stress is proportional to it, thereby dissipating energy instantaneously by viscous resistance. On the other hand, complex fluids and gels, whose components are usually long macromolecules suspended in a viscous solvent, exhibit *viscoelasticity*, i.e. both viscous (liquid-like) and elastic (solid-like) responses are possible [4]. Therefore, they are able to store and dissipate energy depending on the time-scale of observation. The goal of rheology is to provide quantitative parameters, e.g. viscosities, relaxation moduli and creep compliences, that relate the stress and the strain (or the strain rate) of the material under deformation. To this end, the most straightforward techniques consist in imposing such parameters in a controlled manner by means of a rheometer to the material sample of interest and then measuring the corresponding mechanical response. Despite their relative simplicity, these methods require typically milliliter-sized sample volumes, thus being unsuitable for soft matter systems which are expensive or difficult to find in abundance, such as biological fluids and newly synthesized materials.

Microrheology overcomes this major drawback by measuring mechanical properties of a soft material sample using colloidal probes directly embedded in it. The probe particles have the possibility of being manipulated by optical tweezers [3, 5], thus tailoring the forces that can be exerted to locally strain the sample, as depicted in Fig. 1(a). The rheological information of the material is fully inferred from the motion of the probe, which requires only the detection and tracking of its position over time. Therefore, very small sample amounts, typically ranging from pico to microliters, are needed. This in turn allows to carry out *in situ* rheological measurements which are inaccessible to macro-

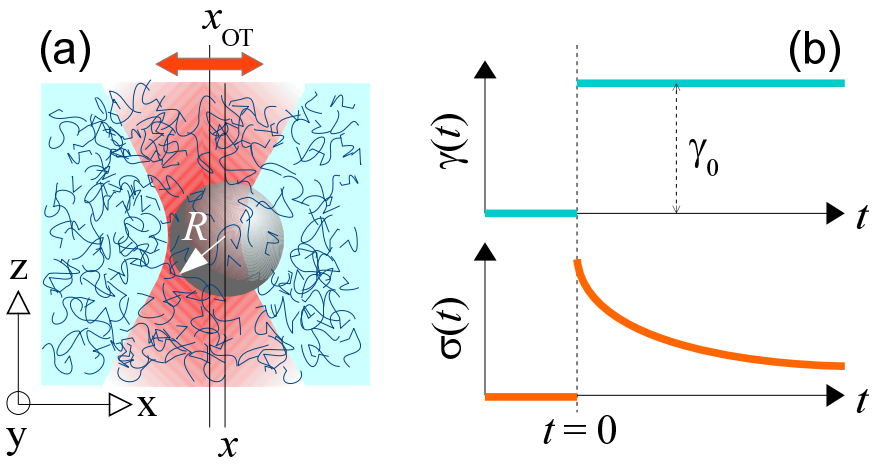

Figure 1: (a) Sketch of the typical experimental system used in Microrheology. A spherical colloidal bead (radius R), embedded in a soft material, is trapped by optical tweezers. If the position of the trapped is fixed, ($x_{\rm OT} = 0$, Passive Microrheology), the particle is only subject to the thermal collisions of the components of the surrounding fluid microstructure. If $x_{\rm OT}$ is varied in time, an additional time-dependent force is exerted on the probe particle (Active Microrheology). (b) Sketch of the response of the shear stress $\sigma(t)$ of a viscoelastic material to a step-like shear strain $\gamma(t)$. For $t \geq 0$, the ratio $\sigma(t)/\gamma_0$ defines the stress relaxation modulus $G(t)$.

scopic methods, e.g. biofluids within living tissues and cells, soft interfaces and membranes. Furthermore, Microrheology offers several advantages over conventional macroscopic rheometry. For instance, unlike bulk rheology, which provides quantities averaged over the entire macroscopic sample, Microrheology permits to explore local mechanical properties at the length-scale of the micron-sized probe. This is particularly useful for investigating heterogeneous materials and fluids close to interfaces, where submillimetric spatial variations of the rheological parameters occur. In addition, undesirable artifacts that can arise due to inertial effects when using a macroscopic rheometer are automaticaly ruled out in microrheology due to the extremely low Reynolds numbers ($Re \lesssim 10^{-3}$) of the flows induced by the motion of a micron-sized probe. This expands significantly the available frequency range over which the rheological parameters of the system can be determined without inertial corrections (up to MHz). Moreover, the typical forces and energies involved in microrheology, either from the thermal motion of the material molecules or those externally exerted by optical tweezers, are of order pN and k_BT, respectively. This guarantees that the microstructure of the sample is not irreversibly destroyed by the motion of the probe.

In order to extract meaninful information by means of standard microrheo-

logical methods, some experimental conditions must be fulfilled. First of all, the material must be homogeneous and isotropic at the scale of the probe, which is usually valid when the relevant length-scale of the material, e.g. the mesh size of gels and semidilute polymer solutions, is much smaller than the probe size. In such a case, the environment behaves as a continuum and its mechanical response can be fully characterized by a single scalar function, e.g. the stress relaxation modulus $G(t)$. We point out that, upon applying a step-like shear strain at $t = 0$ to a material, $\gamma_0\Theta(t)$, where Θ is the Heaviside function, this quantity is defined as $G(t) = \sigma(t)/\gamma_0$ for $t \geq 0$, as illustrated in Fig. 1(b). For a *viscoelastic liquid*, $G(t)$ decays to zero over a finite time, while for a *viscoelastic solid*, it decays to a constant non-zero value. In both cases, the drag force experienced by an embedded particle can be written as $\int_{-\infty}^{t} \mathrm{d}t'\Gamma(t-t')\dot{\mathbf{r}}(t')$. Here, $\dot{\mathbf{r}}(t')$ is the instantaneous particle velocity at time t', whereas Γ is a memory function related to $G(t)$, which weights the role of the previous history of the particle motion on its current drag force due to the temporal correlations induced by the surrounding medium. For example, for a spherical particle of radius R, the memory function is $\Gamma(t) = 6\pi RG(t)$, which can be regarded as generalization of the Stokes' law. For a Newtonian fluid with shear viscosity η, the relaxation modulus is $G(t) = 2\eta\delta(t)$, which corresponds to an instantaneous response of the drag force $6\pi\eta\dot{\mathbf{r}}(t)$ to the particle velocity $\dot{\mathbf{r}}(t)$. Moreover, for some techniques it is often required that the sample is in thermal equilibrium and that the forces externally applied to the probe are small enough to keep the material in the linear response regime. Under such conditions, the time evolution of a single particle coordinate, x, is described by a Generalized Langevin equation [6]

$$0 = -\int_{-\infty}^{t} \mathrm{d}t'\Gamma(t-t')\dot{x}(t') - k[x(t) - x_{\mathrm{OT}}(t)] + \zeta(t) \tag{1}$$

In Eq. (1), x_{OT} represents the x-component of the central position of the optical trap (stiffness k), while ζ is a Gaussian noise of zero-mean, $\langle\zeta(t)\rangle = 0$, and autocorrelation $\langle\zeta(t)\zeta(t')\rangle = k_BT\Gamma(|t-t'|)$.

Depending on how optical tweezers are employed to manipulate a colloidal probe embedded in a soft material, two kinds of microrheological techniques exist: *passive* and *active* [1, 2]. In the following subsections, we describe them in more detail and present some basic applications to determine rheological parameters of simple liquids as well as a prototypical viscoelastic fluid: an equimolar wormlike micellar solution made of the surfactant cetylpyridinium chloride (CPyCl) and the salt sodium salicylate (NaSal) in water as a solvent. In order to prepare this viscoelastic fluid, overnight mixing of the two components in deionized water is required at aproximately 320 K, after which a homogenous and isotropic viscoelastic fluid results. Depending on the surfactant/salt concentration, different kinds of microstructures in the aqueous solvent are formed [7]. For instance, above the first critical micelle concentration but below 4.5 mM, the surfactant molecules aggregate into spherical micelles of radius 2-3 nm, which result in a weak viscoelastic behavior of the dilute solution. Increasing

further the concentration up to 10 mM, the surfactant molecules self-organize in flexible cylindrical micelles, which form and deform dynamically in the solvent. Such wormlike micelles have a diameter from 2 to 3 nm, a contour length ranging from 100 nm to 1 μm and the corresponding persistence length and mesh size are of order 10 nm for concentrations between 5 and 10 mM. In this semidilute regime, the fluid is strongly viscoelastic. Then, similar to common optical-tweezer experiments, a very small amount of micron-sized beads must be suspended in a microliter volume of solution. Special care is needed to avoid air bubbles inside the fluid, which can be easily formed due to the presence of the surfactant. Sonication during a few minutes of the fluid with the dispersed colloidal particles is recommended before making the sample cell (see *Section Getting Started?*). During the measurements, the fluid sample must be kept thermally coupled to a thermostat, as the rheological properties of the fluid strongly depend on temperature.

0.1.1 Passive Microrheology

Passive Microrhelogy is the simplest kind of method to implement for the study of the local mechanical response of soft matter. As its name suggests, the embedded colloidal bead is used as a passive element, whose thermal Brownian motion provides all the necessary information to extract, via fluctuation-dissipation relations, the frequency-dependent rheological parameters of the material under investigation. In order to prevent sedimentation as well as a significantly large diffusive displacement of the probe from its initial position, which would otherwise restrict the measurement time of the particle position x, a static optical trap can be used to confine the particle motion around a mean fixed position. Here we present two direct applications of Passive Microrheology with optical tweezers for viscous and viscoelastic liquids.

Determination of zero-shear viscosities. For Newtonian liquids, the autocorrelation function of the particle position provides a straightforward way to determine their viscosities η. From Eq. (1), using the instantaneous memory function $\Gamma(t) = 2\gamma\delta(t)$ for a purely viscous liquid, an expression for such autocorrelation function can be readily derived

$$\langle x(t)x(0)\rangle = \frac{k_B T}{k} e^{-\lambda t}, \quad t \geq 0, \tag{2}$$

where $\langle \ldots \rangle$ represents an ensemble average over different realizations of the thermal noise, while λ is a decay rate related to the viscous friction coefficient γ of the probe and the trap stiffness k: $\lambda = k/\gamma$. In practice, the ensemble average can be replaced by a time average along the stochastic trajectory $x(t)$, provided that the total measurement time of $x(t)$ is much larger than λ^{-1}. On the other hand, for a spherical particle of radius R, the friction coefficient is $\gamma = 6\pi R\eta$, where η is the fluid viscosity. Then, once the trap stiffness k is known (e.g. by the equipartition method: $k = \frac{k_B T}{\langle x(0)^2 \rangle}$, see *Section Calibration?*), the experimental autocorrelation function of x can be fitted to the right-hand side of

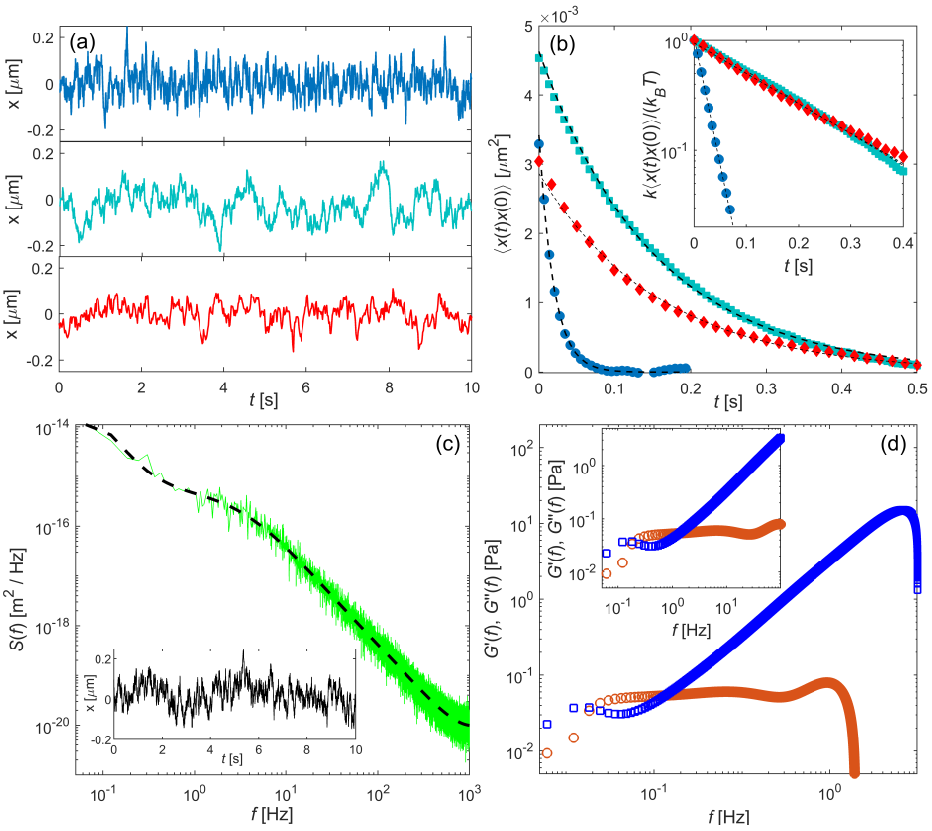

Figure 2: (a) Trajectories of particle of distinct diameter trapped in different fluids. From top to bottom: water ($2R = 2.73\,\mu$m), PNP ($2R = 3.25\,\mu$m) and aqueous miceller solution of CPyCl/NaSal at 4 mM ($2R = 3.25\,\mu$m). (b) Autocorrelation function of the particle position x trapped in the three different cases: water ($\circ$), PNP ($\square$) and micellar solution ($\diamond$). The dashed lines correspond to an exponential fit. Inset: semilog representration of the position autocorrelation function for the three cases, normalized by their corresponding variances $\langle x(0)^2\rangle = \frac{k_B T}{k}$. (c) Power spectral density of equilibrium fluctuations of x for a particle trapped by optical tweezers in wormlike miceller solution of CPyCl/NaSal at 5 mM. Inset: time evolution of x over 10 s. (d) Storage ($\circ$) and loss ($\square$) modulus of the wormlike micellar solution determined by Passive Microrheology. Inset: Expanded view at intermediate frequencies.

Eq. (2). Therefore, η can be determined from the fitting parameter λ by means of $\eta = \frac{k}{6\pi R\lambda}$. This is illustrated in Fig. 2, where the viscosities at $T = 25°\mathrm{C}$ of two Newtonian fluids, water and propylene glycol n-propyl ether (PNP), are computed by means of this passive method. In Fig. 2(a) we plot the typical trajectories x of particles embedded in these liquids, trapped by optical tweezers at approximately $40\,\mu$m away from the cell walls. The corresponding autocorrelation functions of x are shown in Fig. 2(b), where we show that the experimental data (symbols) can be very well fitted to Eq. (2) (dashed lines). (Plots and fits computed with MATLAB routine PosAutocorrelationFunction.m) From the equipartition relation, we first determine the values of the trap stiffness for each case: $k = 1.24 \times 10^{-6}$ N m^{-1} for the particle in water (diameter $2R = 2.73\,\mu$m) and $k = 0.90 \times 10^{-6}$ N m^{-1} for the one in PNP (diameter $2R = 3.25\,\mu$m). Next, from the fitting parameters λ, we find the corresponding values of the viscosities of both fluids: 0.9 mPa s for water and 4.5 mP s for PNP, which agree very well their bulk values.

This technique can be extended to determine steady-state flow properties of viscoelastic *fluids*, which exhibit both liquid- and solid-like responses at times shorter than a typical time τ, as sketched in Fig. 1(b). Such a time-scale reflects the stress relaxation of the elastic material microstructure suspended in the solvent. For a viscoelastic micellar solution, τ originates from the continuos formation and breaking of the micelles as well as their reptation modes for the wormlike structures, and can range from a few milliseconds to several seconds in the semidilute regime [8]. We point out that, unlike viscoelastic *solids* (e.g. gels) these materials are able to flow with constant shear rate at sufficiently long times, $t \gg \tau$, after applying constant shear stress at $t = 0$. Therefore they are characterized by a zero-shear viscosity η_0, which in absence of a confining potential, leads to a long-time diffusion of an embedded spherical particle, where the diffusion coefficient $\frac{k_B T}{6\pi R\eta_0}$. In presence of an optical trap, from Eq. (1) it can be shown that the position autocorrelation function has the form

$$\langle x(t)x(0)\rangle = \frac{k_B T}{k} A e^{-\lambda t}, \;\; \tau \ll t < \lambda^{-1}, \tag{3}$$

where $A < 1$ is a prefactor that depends mainly on k and τ and $\lambda = \frac{k}{6\pi R\eta_0}$. Eq. (3) is valid provided that $\lambda^{-1} \gg \tau$ [9], which must be verified a posteriori. To fulfill this condition of large time-scale separation, small values of the trap stiffness are needed. In Figs. 2(a) and (b), we illustrate this method for a $2R = 3.25\,\mu$m silica particle suspended in a dilute micellar solution (concentration 4 mM, $T = 295$ K), trapped by optical tweezers with stiffness $k = 1.34 \times 10^{-6}$ N m^{-1}. At this concentration, the typical relaxation times are of order of milliseconds. We check that Eq. (3) is a very good approximation to the experimental autocorrelation function of x, where only the first experimental point slightly deviates from the fit. The fitting parameter $\lambda = 6.3\,\mathrm{s}^{-1}$ yields the value $\eta_0 = 6.9$ mPa s, which is also in agreement with reported bulk measurements.

Determination of storage and loss moduli. The complex shear modulus, $G^*(f) = G'(f)+\mathrm{i}G''(f)$, is a quantity used in rheology to characterize linear viscoelasticity of soft matter. It is closely related to the Fourier transform, $\tilde{G}(f)$, of the stress relaxation modulus, $G(t)$, by means of $G^*(f) = 2\pi\mathrm{i}f\tilde{G}(f)$. Therefore, for an applied oscillatory shear strain $\gamma(f) = \gamma_0 e^{2\pi\mathrm{i}ft}$ with amplitude γ_0 and frequency f, the resulting shear stress is also oscillatory and can be expressed as $G^*(f)\gamma(f)$. Here, $G'(f)$ is called the storage modulus, while $G''(f)$ is the loss modulus, and they account for the elastic energy in phase with the applied strain and the out-of-phase viscous dissipation of the material, respectively. For instance, for a purely viscous liquid (viscosity η), $G'(f) = 0$ and $G''(f) = 2\pi f\eta$, whereas for an elastic solid (elastic modulus G_0), $G'(f) = G_0$, and $G''(f) = 0$. In general, for viscoelastic materials, both storage and loss moduli are non-zero.

A very helpful expression for $G^*(f)$ in terms of the equilibrium fluctuations of the position x of a trapped particle can be derived from the fluctuation-dissipation theorem. The latter relates the linear response function $\chi(t)$ of x to an external perturbative force $F(t)$, e.g. that exerted by the motion of the trap position $F(t) = kx_{\mathrm{OT}}(t)$, defined as

$$\langle x(t)\rangle_F = \langle x(0)\rangle_F + \int_0^t dt'\chi(t-t')F(t'), \tag{4}$$

with the *equilibrium* autocorrelation function of x (in absence of external perturbation $F(t)$), i.e. $\langle x(t)x(0)\rangle$. In Eq. (4), the *nonequilibrium* ensemble average $\langle\ldots\rangle_F$ is defined in presence of the time-dependent perturbation. From Eqs. (1) and (4), the one-sided Fourier transform of $\chi(t)$, $\tilde{\chi}(f) = \chi'(f) + \mathrm{i}\chi''(f)$, can be directly related in frequency domain to the complex shear modulus $G^*(f)$ by means of

$$G^*(f) = \frac{1}{6\pi R}\left[\frac{1}{\tilde{\chi}(f)} - k\right]. \tag{5}$$

Making use of the fluctuation-dissipation theorem in frequency domain and the Kramers-Kronig relations, one can find both the real, $\chi'(f)$, and the imaginary $\chi''(f)$ part of the response function $\tilde{\chi}(f)$

$$\chi'(f) = \frac{2\pi}{k_BT}P\int_0^\infty d\nu\frac{\nu^2 S(\nu)}{\nu^2 - f^2}, \tag{6}$$

$$\chi''(f) = \frac{\pi f}{2k_BT}S(f). \tag{7}$$

where $S(f) = \langle|\tilde{x}(f)|^2\rangle$ is the one-sided power spectral density of x in thermal equilibrium, i.e. the Fourier transform of $\langle x(t)x(0)\rangle$, whereas P denotes the Cauchy principal value of the integral. Thus, once $\chi'(f)$ and $\chi''(f)$ are determined, from Eq. (5), the storage $G'(f)$ and loss $G''(f)$ can be computed over the the available frequency range $[0, f_{max}]$. For a given sampling frequency f_s of $x(t)$, f_{max} is fixed by the Nyquist frequency: $f_{max} = \frac{1}{2}f_s$. Note that this technique needs a rather high sampling frequency of $x(t)$ to avoid a large underestimation of the integral in Eq. (6).

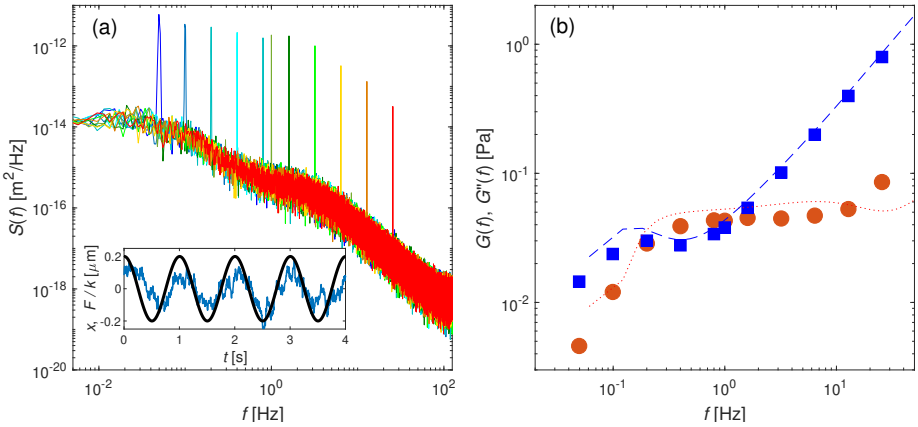

Figure 3: (a) Power spectral density of the particle position, driven at different frequencies by a sinusoidal motion of the optical trap. The peaks are located at the imposed frequencies f_d. Inset: exemplary time evolution of the perturbative force at $f_d = 1$ Hz (thick solid line) and resulting particle position (thin solid line) (b) Numerical values of the storage (•) and loss (■) modulus obtained by means of Equations (5) and (10). The dotted and dashed lines depict the corresponding curves shown in Fig. 2(d) obtained by Passive Microrheology.

In Figs. 2(c) and (d), we apply the previous method to characterize the linear viscoelasticity of the wormlike micellar solution in the semidilute regime at 5 mM. (For this part, the MATLAB script PassiveMicrorheologyKramersKronig.m with functions spectave.m, compspe2.m and KramersKronig.m were used). First, we compute the equilibrium power spectral density $S(f)$ of a long trajectory $x(t)$ measured over 25 min at a sampling frequency $f_s = 2000$ Hz. Since any discrete Fourier transform involved in the calculation of $S(f)$ leads inexorably to a noisy curve, the spectral profile must be smoothed before numerically computing the integral of Eq. (7). In Fig. 2(c) we show the original noisy profile of $S(f)$ (green line) obtained by means of a discrete Fourier transform computed with 2^{17} points. A polynomial fit (solid black line) is performed in order to smooth the power spectral density profile. Then, a direct numerical calculation using Eqs. (5)-(7) leads to the values of the storage and loss moduli shown in Fig. 2(d) over the available frequency interval $0\,\text{Hz} \leq f \leq 1000\,\text{Hz}$. It should be noted that at high frequencies approaching $\frac{1}{2}f_s$, an abrupt decrease of the numerical values of both $G'(f)$ and $G''(f)$ is observed. This is an artifact due to the finite frequency range, which imposes a cut-off in the required Kramers–Kronig integral transformation [10]. Therefore, the physically meaningful values of the components of the complex modulus $G^*(f)$ are only those plotted in the inset of Fig. 2(d), at frequencies one decade below the Nyquist frequency.

0.1.2 Active Microrheology

In Active Microrheology, the trapped colloidal probe is externally forced through the material in order to locally strain it, and its mechanical response to such a perturbation is directly measured [11], from which $G^*(f)$ can be determined by means of Eq (5). Different kinds of perturbations are possible. For instance, the probe particle can be trapped by static optical tweezers while the whole sample cell is moved by a piezo stage (see Sect *Active Calibration?*), or a time-dependent electric field can be applied to the trapped bead. Here, we will only focus on a perturbation created by the oscillatory motion of the position $x_{\mathrm{OT}}(t)$ of the optical trap, which exerts a time-dependent force $F(t) = kx_{\mathrm{OT}}(t)$ on the particle according to Equation (1). As Active Microrheology provides a direct measurement of the linear response function $\chi(t)$ defined in Eq. (4), it does not necessarily require that the material under investigation is in thermal equilibrium. Consequently, this kind of technique it is suitable for the investigation of rheological properties of general viscoelastic fluids and solids, including out-of-equilibrium soft matter, such as actin networks [12, 13], and glassy colloidal suspensions [14]. It is particularly useful for the determination of the storage $G'(f)$ and loss $G''(f)$ modulus at a specific driving frequency f_d, for which an single-frequency oscillatory perturbation force

$$F(t) = kX_0 \cos(2\pi f_d t + \phi), \tag{8}$$

can be directly applied to the colloidal probe, where X_0 is the maximum displacement of the optical trap and ϕ is the initial phase. Therefore, a previous passive calibration of k is needed to know the applied force (see *Section Calibration?*). In order for both the optical trapping and the material microstructure to remain in the linear response regime, X_0 must be sufficiently small. This is generally fulfilled if the typical energy injected by $F(t)$ is at most of order k_BT, i.e. $X_0 \lesssim \sqrt{k_BT/k}$.

In Figure 3 we show some results to illustrate the implementation of Active Microrheology to characterize the rheological properties of a wormlike micellar solution at 5 mM and $T = 20°\mathrm{C}$. (For this part, the MATLAB script ActiveMicrorheologySinusoidalPerturbation.m was used). In the inset of Figure 3(a) we show the typical time evolution of $F(t)$, which results from the sinusoidal motion of the optical trap, with amplitude $X_0 = 200$ nm, trap stiffness $k = 1.0 \times 10^{-6}$ N m^{-1} and driving frequency $f_d = 1$ Hz, see Eq. (8). We also plot the trajectory $x(t)$ of an actively driven particle ($2R = 2\,\mu$m), which clearly exhibits an oscillatory behavior with a time delay relative to $F(t)$ due the the resistance of the surrounding viscoelastic fluid. Here, the crucial step is to compute the one-sided Fourier transform of the linear response function from the measurement of $x(t)$ and $x_{\mathrm{OT}}(t)$. From Eq. (4), this is given by

$$\tilde{\chi}(f) = \frac{\langle \tilde{x}(f) \rangle_F}{k\tilde{x}_{\mathrm{OT}}(f)}, \tag{9}$$

where the numerator is the value at frequency f of the non-equilibrium ensemble average of the Fourier transform of $x(t)$, in presence of $F(t)$ with the same initial

phase ϕ, whereas the denominator involves the Fourier transform of the trap position. Due to the sinudoidal form of $x_{\rm OT}(t)$, the denominator is zero for all frequencies f different from f_d. Therefore, in practice it is curstomary to compute instead the inverse of Eq. (9) and to approximate it at f_d by

$$\frac{1}{\tilde{\chi}(f_d)} = \frac{k\langle \tilde{x}_{\rm OT}(f_d)\tilde{x}^*(f_d)\rangle_\phi}{\langle |\tilde{x}(f_d)|^2\rangle_\phi} \tag{10}$$

where the numerator is the Fourier transform of the cross-correlation function between the trap position and the particle position, while the denominator is the value of the power spectral density of x, both quantities at frequency f_d, first computed for a given $F(t)$ and then averaged over different realizations of ϕ. In Fig. 3(a) we plot the power spectral density of the particle position x in presence of the force $F(t)$ at different driving frequencies f_d. The pronounced peaks at $f = f_d$ result from the sinusoidal form of $F(t)$, while for $f \neq f_d$, the contribution to $S(f)$ is only due to thermal noise in the fluid. In Fig. 3(b) we plot as symbols the values of the storage and loss modulus computed by means of Equations (5) at the distinct driving frequencies. For comparison, we also represent as dotted and dashed lines the correspoding values determined by Passive Microrheology, showing a rather good agreement between both methods. We would like to emphasize that, although more elaborate to implement in experiments, Active Microrheology is less prone to numerical artifacts than Passive Microrheology. This is because it is based on a measurement of the mechanical response of the particle position at a single frequency, which does not require any indirect numerical integration over a discrete finite frequency interval as those involved in the Kramers-Kronig relations.

0.1.3 Other microrheological applications and outlook

In the previous subsections, we have described some basic applications of Microrheology with optical tweezers. More advanced methods, which are beyond the scope of this tutorial, focus on investigating flow and deformation properties of complex materials which do not trivially fulfill the general conditions described in Subsection 0.1. Some relevant examples are the following:

- *Interfacial Microrheology.* Near a liquid-solid, a liquid-liquid or a liquid-vapor interface, the viscosity of liquids becomes anisotropic and exhibits a dependence on the closest distance to the interface due to the specific hydrodynamic boundary conditions. Passive Microrheology can be applied to determine such a spatial dependence, provided that the three spatial coordinates of the probe particle, embedded in the liquid phase of interest, can be tracked [15, 16].

- *Two-Point Microrheology.* The motion of pairs of colloidal particles not so far from each other is strongly correlated when suspended in a fluid. Since the flow and strain fields around one of them entrain the second particle, the motion of the latter encodes information of the rheological properties

of the fluid at the location of the former. Therefore, a dual-beam optical tweezers can be used to fix their mean separtion and perform the so-called Two-Point Microrheology. Here, one particle plays the role of a control element, either thermally or externally driven, while the second one is used as a passive probe. This technique is particularly useful to investigate the mechanical response of heterogeneous and anisotropic soft materials, such as gels and polymer solutions [17, 18].

- *Transient Microrheology.* Using a combination of both Active and Passive Microrheology, the transient behavior of viscoelastic materials either upon flow startup or cessation can be investigated. For example, during an active period, an optically trapped particle can be driven though the viscoelastic fluid, followed by a sudden release from the tweezers by shutting off the laser, during which its position is recorded. During this non-equilibrium passive period, the particle motion is subject to the recovery of the initially strained fluid microstructure. Consequently, this technique allows to measure in a straightforward manner relaxation times and relaxation moduli of viscoelastic materials [19, 20].

Microrheology has evolved during the last two decades into a powerful experimental tool to investigate complex soft materials. Most of its current applications rely on a well-established theoretical framework based on equilibrium statistical mechanics, low-Reynolds-number hydrodynamics and linear response theory. Nevertheless, more recent approaches aim to investigate non-linear rheological properties, e.g. thinning of polymer solutions, by means of colloidal probes driven at very high velocities or under large-amplitude oscillations [3]. Although the implementation of such microrheological techniques does not represent a big experimental challenge, the interpretation of the data in terms of meaningful parameters and its connection with bulk quantities is not trivial. A complete understanding of such a wealth of information will certainly rely on current theoretical advancements in non-equilibrium soft matter systems [21], which are able to find a direct link between the motion of the probe and the microstructural deformation of the surrounding medium.

References

[1] T. M. Squires and T. G. Mason, Annu. Rev. Fluid Mech. **42**, 413 (2010).

[2] T. A. Waigh, Rep. Prog. Phys. **79**, 074601 (2016).

[3] R. M. Robertson-Anderson, ACS Macro Lett. **7**, 968 (2018).

[4] R. B. Bird, R. C.. Armstrong, and O. Hassager, Dynamics of Polymeric Liquids (Fluid Mechanics), Vol. (John Wiley & Sons, New York, 1987), Vol. 1.

[5] M. Tassieri et al., New J. Phys. **14**, 115032 (2012).

[6] R. Kubo, Rep. Prog. Phys. **29**, 255 (1966).

[7] N. Z. Handzy and A. Belmonte, Phys. Rev. Lett.**92**, 124501 (2004).

[8] M. E. Cates and S. Candau, J. Phys.: Condens. Matter **2**, 6869 (1990).

[9] M. Tassieri, et al., Sci. Rep. **5**, 8831 (2015).

[10] B. Schnurr , F. Gittes , F. C. MacKintosh and C. F. Schmidt , Macromolecules **30**, 7781 (1997).

[11] L. G. Wilson and W. C. K. Poon, Phys. Chem. Chem. Phys., **13**, 10617 (2011).

[12] D. Mizuno, D. A. Head, F. C. MacKintosh, and C. F. Schmidt, Macromolecules **41**, 7194 (2008).

[13] P. Gallet, D. Arcizet, P. Bohec, and A. Richert, Soft Matter **5**, 2947 (2009).

[14] N. Senbil, M. Gruber, C. Zhang, M. Fuchs, and F. Scheffold, Phys. Rev. Lett. **122**, 108002 (2019).

[15] G. M. Wang, R. Prabhakar, and E. M. Sevick, Phys. Rev. Lett. **103**, 248303 (2009).

[16] R. Shlomovitz, A. A. Evans, T. Boatwright, M. Dennin, and A. J. Levine, Phys. Rev. Lett. 110, 137802 (2013).

[17] J. C. Crocker, M. T. Valentine, E. R. Weeks, T. Gisler, P. D. Kaplan, A. G. Yodh, and D. A. Weitz Phys. Rev. Lett. **85**, 888 (2000).

[18] S. Paul, A. Kundu and A. Banerjee, J. Phys. Commun. **3** 035002 (2019).

[19] C. D. Chapman and R. M. Robertson-Anderson, Phys. Rev. Lett. **113**, 098303 (2014).

[20] J. R. Gomez-Solano and C. Bechinger, New J. Phys. **17** 103032 (2015).

[21] R. N. Zia, Annu. Rev. Fluid Mech. **50**, 371 (2018).